Available online at www.sciencedirect.com
SCIENCE DIRECT
Journal of Molecular Catalysis A: Chemical 249 (2006) 240–245
JOURNAL OF MOLECULAR CATALYSIS A: CHEMICAL
www.elsevier.com/locate/molcata

A novel mesoporous oxidation catalyst La-Co-Zr-O prepared by using nonionic and cationic surfactants as co-templates

Zhi-Qiang Zou [a], Ming Meng [a,*], Jin-Yong Luo [a], Yu-Qing Zha [a], Ya-Ning Xie [b], Tian-Dou Hu [b], Tao Liu [b]

[a] *Department of Catalysis Science & Technology, School of Chemical Engineering & Technology, Tianjin University, Tianjin 300072, PR China*
[b] *Institute of High Energy Physics, Chinese Academy of Sciences, Beijing 100039, PR China*

Received 3 November 2005; received in revised form 28 December 2005; accepted 4 January 2006
Available online 23 February 2006

Abstract

The mesoporous La-Co-Zr-O catalyst with the atomic ratio of La + Co/La + Co + Zr = 0.5 was prepared by citric acid complexation-organic template decomposition method, using the mixture of nonionic *p*-octyl polyethylene glycol phenyl ether (OP) and cationic cetyltrimethyl-ammonium bromide (CTAB) as co-templates (LCZ-OP/CTAB-0.5). The results of BET and pore size distribution show that this sample possesses much bigger specific surface area (117.6 m^2/g) than those prepared by using single template CTAB (96.6 m^2/g, LCZ-CTAB) or by using conventional co-precipitation method (21.6 m^2/g, LCZ-CO). Both the samples obtained from single template CTAB and from the co-templates of OP and CTAB show very uniform mesoporous pore diameter (3.5–4.3 nm). The structural characterization results of XRD, XPS and Co K-edge EXAFS indicate that the highly dispersed Co_3O_4 crystallite should be the main active phase for CO oxidation. The crystal sizes of Co_3O_4 crystallites in LCZ-CTAB and LCZ-OP/CTAB-0.5 are 23.4 and 32.5 nm, respectively, which are much smaller than that in LCZ-CO (56.8 nm). The catalytic activity evaluation shows that the sample prepared by co-templates decomposition possesses much better activity for CO oxidation, especially the low temperature oxidation activity. However, the activity sequence of the samples is not the same as the crystal size of Co_3O_4 phase. On the contrary, the reducibility of bond Co–O and the reduced amount of Co_3O_4 phase below 500 °C for the samples are well correlated with their activity law, which should be a crucial factor for the oxidation performance of the samples.

Keywords: Mesoporous La-Co-Zr-O catalyst; Cetyltrimethyl-ammonium bromide (CTAB); *p*-Octyl polyethylene glycol phenyl ether (OP); Structural characterization; CO oxidation

1. Introduction

In order to control the automobile exhaust pollution, more and more researchers are endeavoring to develop novel catalysts applicable to the exhaust device. Up to now, the three-way catalysts (TWCs) have been successfully developed to remove the CO, NO_x and hydrocarbons in the gasoline engine exaust during the normal running period [1], however, these catalysts show very low efficiency for the oxidation of CO and hydrocarbons during the cold start period because of the much lower temperatures of the catalyst-bed and exaust (<200 °C), which results in the release of 60–80% of the CO and hydrocarbons in the exaust into the air [2]. So, it is very necessary to explore novel oxidation catalysts for the removal of CO and hydrocarbons at relatively low temperature.

It has been reported that the cobalt-based catalysts are active for many catalytic reactions, such as Fischer–Tropsch synthesis [3], NO decomposition and selective reduction [4–8], and the oxidation of CO and hydrocarbons [9]. Lanthanum and zirconium oxides are sometimes added to the catalysts as excellent promoters to improve the dispersion and increase the surface area [10–12]. So, it is a feasible idea to develop a catalyst containing La, Co and Zr. It is well known that perovskite type oxides containing transition metals (e.g., Co, Cr, Mn, etc.) often show high activity for the total oxidation of hydrocarbons and CO [13,14]. However, these materials usually possess low specific surface areas after calcination at high temperature. Recently, much attention is attracted to the mesoporous materials with

* Corresponding author. Tel.: +86 22 2789 2275; fax: +86 22 2740 5243.
E-mail address: mengm@tju.edu.cn (M. Meng).

1381-1169/$ – see front matter © 2006 Elsevier B.V. All rights reserved.
doi:10.1016/j.molcata.2006.01.010

large specific surface areas and uniform pore sizes. The most reported mesoporous catalysts are based on Si, Al-Si and Ti-Si molecular sieves, such as MCM-41, MCM-48, TS-1, etc. [15–19], which normally show no catalytic activity and just serve as support. In our present study, the method of preparing mesoporous Si-containing molecular sieves was used for reference to prepare the mesoporous nonsilica mixed oxide catalysts La-Co-Zr-O, and the mixture of the nonionic *p*-octyl polyethylene glycol phenyl ether (OP) and cationic cetyltrimethyl-ammonium bromide (CTAB) was used as co-templates. The oxidation property of this catalyst is much better than that obtained by co-precipitation method and that by using single CTAB as template. The techniques of nitrogen adsorption/desorption (NAD), X-ray diffraction (XRD), X-ray photoelectron spectroscopy (XPS), the extended X-ray absorption fine structure (EXAFS) and the temperature-programmed reduction by H_2 (H_2-TPR) were used for the characterization of the catalysts. The correlation between the catalyst structures and the catalytic activities for CO oxidation is discussed.

2. Experimental

2.1. Catalyst preparation

At first, the La-Co citrate complex precursor were prepared from 2.15 g of lanthanum nitrate, $La(NO_3)_3{\cdot}6H_2O$, 1.45 g of cobalt nitrate, $Co(NO_3)_2{\cdot}6H_2O$ (atomic ratio Co/La = 1) and 1.92 g of citric acid [13]. The cetyltrimethyl-ammonium bromide (7 g) was dissolved in 120 g distilled water and 30 g of HCl 10 wt%. Then the La-Co citrate complex precursor and 4.28 g of zirconium nitrate (atomic ratio La + Co/La + Co + Zr = 0.5) dissolved in distilled water were added, giving a clear homogeneous solution. The mixture was continuously stirred for 2 h. Then 80 ml of 2 M NaOH was quickly added with vigorous stirring to form a solid precipitate. The pH was adjusted to 12.5. The resulting gel mixture was stirred for 6 h at room temperature and subsequently heated to 95 °C and kept at this temperature for 48 h to increase the degree of condensation. The solid product was filtered, washed with ethanol, dried in air at 110 °C and finally calcined in air at 500 °C for 8 h. This catalyst is denoted as LCZ-CTAB, where LCZ = La-Co-Zr oxides. The next sample was prepared by using co-templates of OP and CTAB. The procedure is the same as that for LCZ-CTAB but the template is replaced by the mixture of OP and CTAB with the molar ratio of OP/CTAB = 0.5, and the whole molar amount of the mixed templates is the same as the CTAB used in LCZ-CTAB preparation. The corresponding catalyst is denoted as LCZ-OP/CTAB-0.5. For comparison, another sample with the same composition of La, Co and Zr was prepared by conventional co-precipitation, which is denoted as LCZ-CO.

2.2. Nitrogen adsorption/desorption

The measurement of the specific surface area (S_{BET}) and the pore diameter distribution were carried out at 77 K on a SORPTOMATIC 1990 SERIES apparatus (Thermo-Finnigan) by using the nitrogen adsorption/desorption method. The samples were pretreated in vacuum at 200 °C for 8 h before experiments. The specific area (S_{BET}) was determined from the linear part of the BET curve. The pore diameter distribution was calculated from the desorption branch of N_2 adsorption/desorption isotherms using the Barrett–Joyner–Halenda (BJH) formula.

2.3. X-ray diffraction

XRD patterns were recorded on an X'pert Pro diffractometer (PANAlytical Company) with a rotating anode using Co Kα as radiation source (λ = 1.7902 Å). The data of 2θ from 20 to 80° range were collected with the step size of 0.02°.

2.4. X-ray photoelectron spectroscopy

XPS analysis was performed in a PHI-1600 ESCA SYSTEM spectrometer (XPS) with Mg Kα as X-ray source (1653.6 eV) under a residual pressure of 5×10^{-6} Pa. The error of the binding energy is ±0.2 eV and the C1s (E_b = 284.6 eV) of the contaminated carbon was used as a standard for binding energy calibration.

2.5. Extended X-ray absorption fine structure

Co K-edge (7709.7 eV) EXAFS spectra were recorded on the EXAFS station, 1W1B beam line of Beijing Synchrotron Radiation Facility of National Laboratory (BSRF NL). The critical beam energy was 2.2 GeV with a storage ring current of ~80 mA. The transition mode was used to record the data. A Si(1 1 1) double-crystal monochromator was used to reduce the harmonic content of the monochromator beam. The background-subtracted EXAFS function was converted into *k* space and weighted by k^3 in order to compensate for the diminishing amplitude due to the decay of the photoelectron wave. The EXAFS structural parameters of samples were obtained by curve-fitting. Co_3O_4 and $LaCoO_3$ were used as model compounds.

2.6. Temperature-programmed reduction

TPR measurement was conducted on a TPDRO 1100 apparatus supplied by Thermo-Finnigan company. Each time, 30 mg of the sample was heated from room temperature to 900 °C at a rate of 10 °C/min. A mixture gas of H_2 and N_2 (H_2/N_2 molar ratio: 5%) was used as reductant with a flow rate of 20 ml/min.

2.7. Evaluation of catalytic performance

The catalytic activities of the samples for CO oxidation were measured in a fixed-bed quartz tubular reactor (i.d. 8 mm) mounted in a tube furnace. The reactant is a mixture gas, which contains 1.1% CO and 4.7% O_2 (molar percentage), balanced with pure N_2. The gas hourly space velocity (GHSV) is 6400 h^{-1}. The effluent gas from the reactor was analyzed by a gas chromatograph (BFS, SP 3430) equipped with a TCD detector.

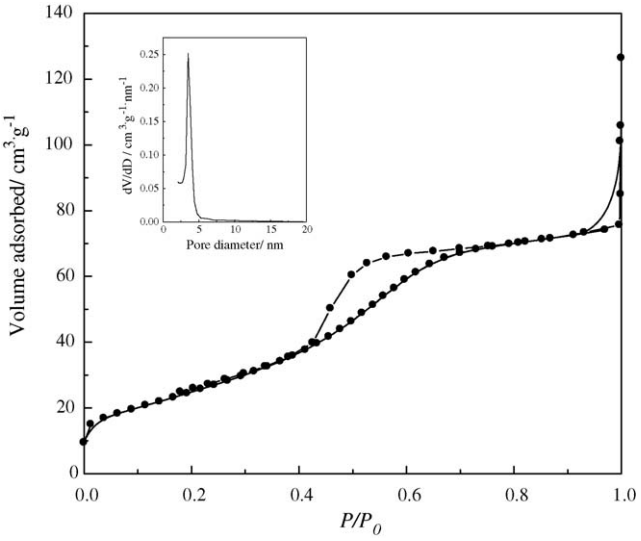

Fig. 1. Nitrogen adsorption/desorption isotherm and pore diameter distribution (inset) of LCZ-CTAB.

3. Results and discussion

3.1. Specific surface area and pore diameter distribution

The nitrogen adsorption/desorption isotherm of LCZ-CTAB is shown in Fig. 1, which exhibits a typical IV shape as defined by IUPAC [20]. From Fig. 1, it can be seen that the P/P_0 position of the inflection point is related to a diameter in the mesopore range, and that the BJH pore size distribution is very narrow, which is from 3.5 to 3.8 nm (Fig. 1, inset), implying the textural uniformity of the sample. Furthermore, the specific surface area of LCZ-CTAB ($S_{BET} = 96.6\ m^2/g$) is much bigger than the sample prepared by co-precipitation LCZ-CO ($S_{BET} = 21.6\ m^2/g$). The nitrogen adsorption/ desorption isotherm of the sample obtained by using co-templates of CTAB and OP (LCZ-OP/CTAB-0.5) is shown in Fig. 2. It is similar to that of LCZ-CTAB but the specific surface area is further increased to $117.6\ m^2/g$ and the range of pore size distribution becomes a little broader (3.5–4.3 nm). In our synthesis experiment, the same surfactants were used as in the literature [21], if the formation mechanism of micella is similar to the literature, the effect of the surfactants on the specific surface area and pore diameter may be explained by the surfactant packing parameter, $g = V/(a_0L)$, where V is the total volume of the surfactant chains, a_0 is the effective head group area at the organic–inorganic interface and L is the kinetic surfactant chain length. The polar part of the nonionic surfactant OP used in LCZ-OP/CTAB-0.5 is a polymer $-(EO)_n$ with a big volume. When it is tied in the micella formed by CTAB, it will minish the curvature of the polar part of the micella and then the value of a_0 will decline. Furthermore, the hydrophobic part of OP has not only an alkyl chain but also a phenyl ring with a π electron, which has stronger dispersive ability than alkyl chains, so the hydrophobic part of OP can interact with the hydrophobic alkyl chains of the micella formed by CTAB. Therefore, partial OP may be embedded in the interspace of the micella formed by CTAB, which increased the total volume of the surfactant chains (V) of the micella. Due to the two factors the surfactant packing parameter g will increase and the pore size of the corresponding catalysts will increase consequently.

3.2. XRD

XRD patterns of LCZ-CTAB, LCZ-OP/CTAB-0.5 and LCZ-CO are shown in Fig. 3. In contrast with the normative diffraction peaks of ZrO_2 ($2\theta = 35.1$, 59.0, 40.8 and 70.7°), the diffraction peaks of ZrO_2 in all the samples shift to lower angles, suggesting a little increase of the interplanar d spacing. This may be resulted from the entering of La^{3+} into the crystal lattice of ZrO_2, whose radius (0.118 nm) is bigger than Zr^{4+} (0.084 nm). The diffraction peaks of the samples obtained by organic templates decomposition are much lower and wider than the sample prepared by co-precipitation method, which means that the crystal sizes of the components in the former catalysts

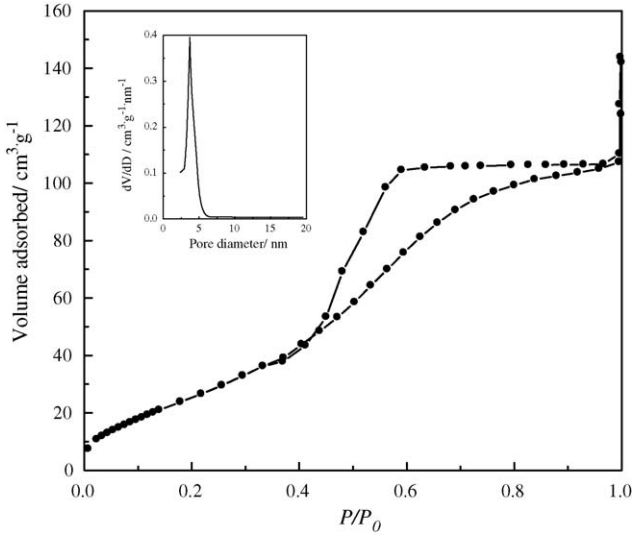

Fig. 2. Nitrogen adsorption/desorption isotherm and pore diameter distribution (inset) of LCZ-OP/CTAB-0.5.

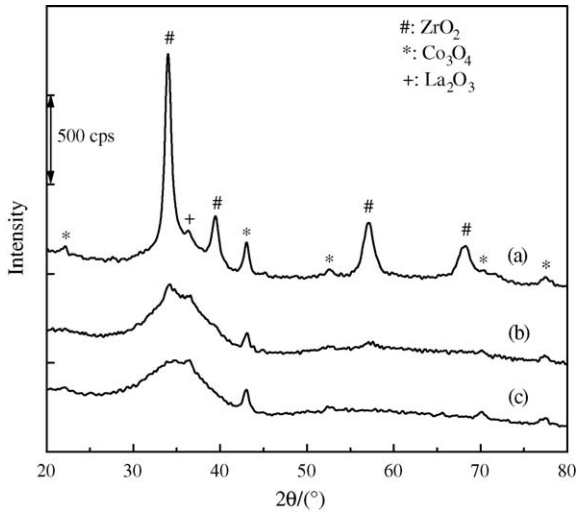

Fig. 3. The XRD patterns of the samples: (a) LCZ-CO, (b) LCZ-CTAB and (c) LCZ-OP/CTAB-0.5.

Table 1
The XPS results of the samples

Sample	Binding energy (eV)				Surface atomic percentages (%)		
	O 1s	Co $2p_{3/2}$	La $3d_{5/2}$	Zr $3d_{5/2}$	La	Co	Zr
LCZ-CO	530.8	779.5	833.6	181.4	12.5	15.0	72.5
LCZ-CTAB	530.7	779.8	834.2	181.5	16.0	27.2	56.8
LCZ-OP/CTAB-0.5	530.2	779.8	834.5	181.9	16.7	18.8	64.6

are much smaller. The crystal size of Co_3O_4 crystallite in LCZ-CTAB, LCZ-OP/CTAB-0.5 and LCZ-CO is about 23.4, 32.5 and 56.8 nm, respectively, which are obtained by Scherrer Equation on the basis of reflection [3 1 1] ($2\theta = 43.1^\circ$). By comparison of the XRD peaks of ZrO_2 in LCZ-OP/CTAB-0.5 and LCZ-CTAB, it can be found that the crystal size of ZrO_2 in sample LCZ-OP/CTAB-0.5 is smaller than that in sample LCZ-CTAB. Since zirconium oxide is the main component in the samples, its size should have a big effect on the specific surface area of the samples. This deduction is a good explanation for the bigger BET area of LCZ-OP/CTAB-0.5 than LCZ-CTAB.

3.3. XPS

XPS analysis was performed in order to gain the binding energy and percentages of surface atoms. The results are listed in Table 1. From Table 1, it can be seen that the binding energy of cobalt is in the range of 779.5–779.8 eV, indicating the Co species in all the samples are Co_3O_4 according to literature [22,23]. The percentages of surface atoms La and Co in the sample LCZ-CO are the lowest among the three samples, which is related to the crystal sizes of La and Co-containing phases. The number of atom La in the sample LCZ-CTAB is almost the same as that in the sample LCZ-OP/CTAB-0.5, while the percentage of Co is quite different in the two samples and it is bigger in LCZ-CTAB than in LCZ-OP/CTAB-0.5. All these results show that the amounts of surface La and Co are the lowest in the sample obtained by co-precipitation, which may be due to a correspondingly low dispersion of the La and Co-containing phases. In sample LCZ-CTAB, the amount of surface Co is the highest, which is in good agreement with the smallest crystal size of Co_3O_4 in this sample obtained by Scherrer Equation from XRD results.

3.4. EXAFS

The radial structure functions of Co K-edge of the samples and the model compounds $LaCoO_3$ and Co_3O_4 are shown in Fig. 4. The RSFs of the three samples quite resemble that of Co_3O_4 with four coordination peaks at approximately 0.16, 0.25, 0.31 and 0.47 nm. The first peak is assigned to coordination shell Co–O and the second peak corresponds to coordination shell Co–Co. Comparing the RSFs of the samples and model compounds, it is clear that the main Co species in the samples are Co_3O_4 phases. The structural parameters of the first shells of the model compounds and catalyst samples are listed in Table 2. From Table 2, it can be seen that the coordination number (N) for the first Co–O shell in the samples obtained by using organic templates method is much smaller than that in the sample prepared by co-precipitation method, suggesting the smaller crystal size of Co phases in the former samples. The order for the coordination numbers of Co–O for the three samples is consistent with that of the crystal sizes obtained from XRD results. The coordination distances (R) of Co–O for the samples are almost the same as that of Co_3O_4, indicating that no other complex oxide species, such as $LaCoO_3$, are formed.

3.5. H_2-TPR

The H_2-TPR profiles of the samples are shown in Fig. 5. Normally, La_2O_3 cannot be reduced by H_2, Co_3O_4 can be reduced below 500 °C [22], and ZrO_2 can be reduced above 500 °C, which is attributed to the reduction of a small quantity of Zr^{4+} to

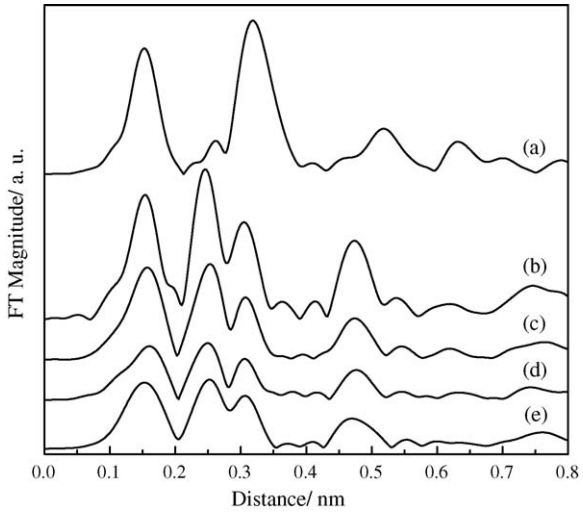

Fig. 4. The radial structure functions of Co K-edge of the samples: (a) $LaCoO_3$, (b) Co_3O_4, (c) LCZ-CO, (d) LCZ-CTAB and (e) LCZ-OP/CTAB-0.5.

Table 2
Best-fitting values of the structural parameters for the first coordination shell Co–O from EXAFS data

	Shell	N	R (nm)	$\Delta\sigma^2$ (nm^2)
Co_3O_4[a]	Co–O	5.3	0.192	
LCZ-CO	Co–O	5.3	0.191	0.000005
LCZ-CTAB	Co–O	4.5	0.191	0.000031
LCZ-OP/CTAB-0.5	Co–O	5.0	0.191	0.000024

[a] The parameters of Co_3O_4 is taken from Ref. [24].

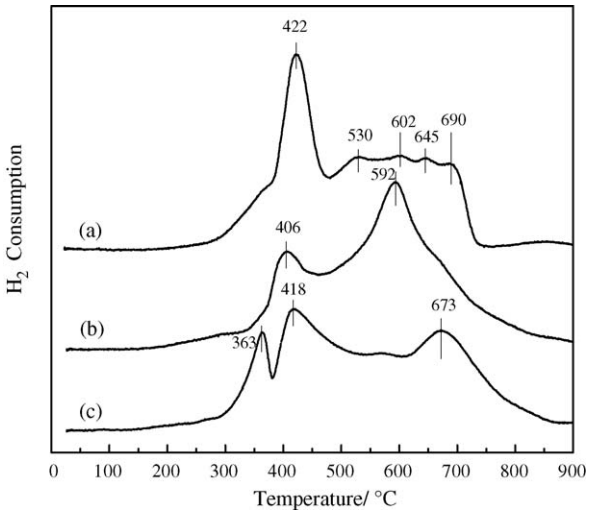

Fig. 5. The H_2-TPR profiles of the samples: (a) LCZ-CO, (b) LCZ-CTAB and (c) LCZ-OP/CTAB-0.5.

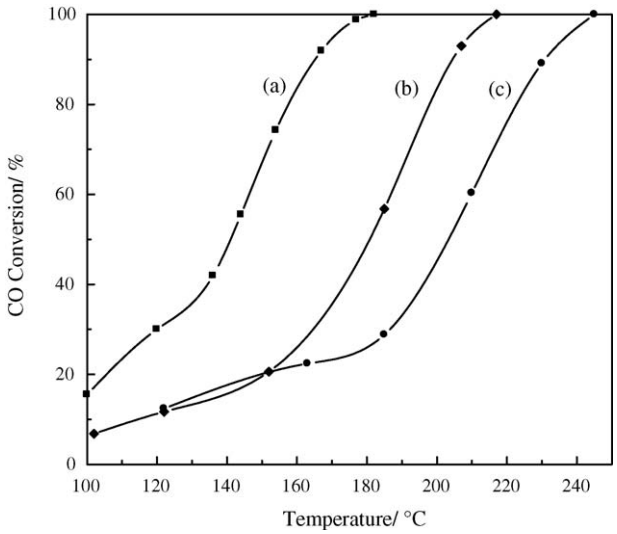

Fig. 6. The CO conversion curves of the samples: (a) LCZ-OP/CTAB-0.5, (b) LCZ-CTAB and (c) LCZ-CO.

Zr^{3+} on the surface or the subsurface of ZrO_2 [25]. To confirm the reduction of cobalt phase, the fresh sample LCZ-OP/CTAB-0.5 was selected to perform partial reduction experiment in the same condition of H_2-TPR from room temperature to 500 °C, after cooling down to room temperature, the XRD pattern of this sample was recorded (not shown). The results show that after partial reduction, the Co_3O_4 phase has transformed into CoO phase. Therefore, in Fig. 5, the peaks below 500 °C could be assigned to the reduction of Co_3O_4 to CoO. While the peaks in high temperature region (>500 °C) should correspond to the reduction of ZrO_2 ($Zr^{4+} \rightarrow Zr^{3+}$) and Co–Zr interacting phases, including the partial reduction product CoO. In most cases, the reduction peak of ZrO_2 ($Zr^{4+} \rightarrow Zr^{3+}$) is very small, here it may be covered by the reduction peaks of Co–Zr interacting phases.

In low temperature region (<500 °C), the reduction temperature of the sample LCZ-CO is the highest among the three samples, which may be resulted from the much larger size of Co_3O_4 crystallite. Comparing the reduction peaks of LCZ-CTAB and LCZ-OP/CTAB-0.5 in this region, it is found that the peak area below 500 °C for LCZ-OP/CTAB-0.5 is much bigger than that for LCZ-CTAB, and there is a peak appearing at much lower temperature (363 °C), suggesting the different chemical surroundings and reducibility of Co_3O_4 phases in these two samples. For the same oxide species, the lower reduction temperature, the easier activation of bond metal–oxygen (Co–O). These factors are tightly related to oxidation performance of the catalysts.

In the high temperature region (>500 °C), the peak should be mainly connected to the reduction of interacting phases between Co and Zr oxide. It is indicated by Sanchez and Gazquez [26] that there are some oxygen vacancies on the surface of ZrO_2 with fluorite structure, which can be occupied by the supported metal ions. After high temperature calcination, Co ions may have occupied the oxygen vacancies or embedded into the fluorite structure of ZrO_2, all these make the reduction of the interacting Co–Zr phases more difficult than normal Co oxide phases. The interacting phases possess very high stability, whose metal–oxygen bond is more difficult to be activated and therefore contribute very little to oxidation activity.

3.6. Catalytic performance for CO oxidation

The catalytic activities for CO oxidation of the samples are shown in Fig. 6. From Fig. 6, it can be seen that the samples obtained by organic templates decomposition method, especially the sample LCZ-OP/CTAB-0.5, show much higher catalytic activity for CO oxidation than the sample prepared by co-precipitation method. The temperature for the full conversion of CO on LCZ-OP/CTAB-0.5 is about 60 °C lower than that on LCZ-CO. In view of the above characterization results, the main reasons for the difference of the activities can be described as follows. Firstly, the samples obtained by organic templates decomposition possess higher specific surface areas and uniform mesoporous sizes, which are in favor of the mass transfer and the contact of reactants with active sites. Secondly, the La and Co-containing phases in the samples obtained by organic templates decomposition have a much higher dispersion in contrast to LCZ-CO. The smaller crystal size of active phase Co_3O_4 and the bigger percentage of surface Co atoms in the former catalysts provide more active sites for the reaction. Finally, the H_2-TPR results show that in the low temperature region (<500 °C), the active phase Co_3O_4 in the samples LCZ-CTAB and LCZ-OP/CTAB-0.5 is reduced at lower temperatures than that in LCZ-CO, indicating that the activation of the Co–O bond in these two samples is easier than that in LCZ-CO, as is helpful to increase the oxidation activities of the catalysts.

Comparing the catalytic activities of the samples LCZ-OP/CTAB-0.5 and LCZ-CTAB, it can be seen that the temperature for the full conversion of CO is about 35 °C lower on LCZ-OP/CTAB-0.5 than on LCZ-CTAB, and that the low temperature oxidation activity of the former catalyst is much better than the later. For example, on LCZ-OP/CTAB-0.5, the CO conversion at 150 °C is about 66%, while it is less than 20% on LCZ-CTAB. These results show that the use of the co-templates

do have a positive impact upon the property of the catalyst, especially the low temperature oxidation activity, which is crucial for the removal of CO and hydrocarbons during the cold start period of vehicles. Considered the crystal sizes of the active phase Co_3O_4 and the percentage of surface cobalt atoms (XRD and XPS results), it is revealed that the catalytic activity of the samples does not totally depend on the crystal size of Co_3O_4 and the surface amount of cobalt atoms. There should be other crucial factors related to the catalytic activities. Firstly, the specific surface area and pore size of sample LCZ-OP/CTAB-0.5 are bigger than those of sample LCZ-CTAB. Secondly, the dispersion of zirconium oxide and the surface atomic percentages of Zr and La in sample LCZ-OP/CTAB-0.5 are higher than those in LCZ-CTAB, which favors the interaction and the cooperation between the active component Co_3O_4 and the oxides of Zr and La. Thirdly, from the results of H_2-TPR, it is discovered that the use of co-templates has largely increased the reduced amount of Co_3O_4 phase below 500 °C, and given rise to a low temperature reduction peak, which means the easier activation and participation of lattice-oxygen (Co–O) in the oxidation-reduction recycle. As a result, that the sample LCZ-OP/CTAB-0.5 exhibits much higher oxidation activity than LCZ-CTAB is natural.

4. Conclusions

(1) The mesoporous mixed oxide catalysts La-Co-Zr-O were successfully prepared by citric acid complexation-organic template decomposition method, which show very uniform mesoporous diameter distribution (3.5–4.3 nm). The sample prepared by using co-templates of *p*-octyl polyethylene glycol phenyl ether and cetyltrimethyl-ammonium bromide possesses much bigger specific surface areas (117.6 m^2/g) than those by using single template CTAB or by co-precipitation method.

(2) The structural characterization results of XRD, XPS and Co K-edge EXAFS show that the main active phase should be Co_3O_4 phases, which have much smaller crystal sizes (23–33 nm) in the samples prepared by organic template decomposition method than in that by co-precipitation method (56.8 nm).

(3) The H_2-TPR results reveal that the reducibility and the reduced amount of Co_3O_4 phase below 500 °C in the sample prepared by using co-templates of OP and CTAB is much larger than those in the sample prepared by using single template of CTAB, which should be one of the crucial factors for the much better oxidation performance of this sample.

Acknowledgements

This work is financially supported by Natural Science Foundation of Tianjin (No.05YFJMJC09700), the Research Foundation for Doctorial Program of the Ministry of Education of China (No.20040056028), and the 985 Program on Education Development of Tianjin University, PR China.

References

[1] T. Kreuzer, E.S. Lox, D. Lindner, J. Leyrer, Catal. Today 29 (1996) 17.
[2] J.C. Summers, J.E. Sawyer, A.C. Frost, ACS Symp. Paper 495 (1992) 98.
[3] E. Iglesia, S.L. Soled, R.A. Fiato, J. Catal. 137 (1992) 212.
[4] M. Shelf, K. Otto, H. Gandh, Atoms. Environ. 3 (1969) 107.
[5] Y. Teraoka, H. Fukuda, S. Kagawa, Chem. Lett. 1 (1990) 1069.
[6] R.J. Voorhoeve, D.W. Johnson, J. Remeika, P.K. Gallagher, Science 195 (1977) 827.
[7] J.M. Tascon, L.G. Tejuca, C.H. Rochester, J. Catal. 95 (1985) 558.
[8] C.H. Hamada, Y. Kintaichi, M. Sasaki, T. Ito, Appl. Catal. 75 (1991) L1.
[9] M. Meng, P.Y. Lin, S.M. Yu, Chin. J. Chem. Phys. 8 (1995) 66.
[10] N. Gunasekaran, S. Saddawi, J.J. Carberry, J. Catal. 159 (1996) 107.
[11] M. Traykova, N. Davidova, J.S. Tsaih, A.H. Weiss, Appl. Catal. A 169 (1998) 237.
[12] K. Sekizawa, H. Widjaja, S. Maeda, Y. Ozawa, K. Eguchi, Catal. Today 59 (2000) 69.
[13] D. Trong On, S.V. Nguyen, S. Kaliaguine, Phys. Chem. Chem. Phys. 5 (2003) 2724.
[14] L.G. Tejuca, J.L. Fierro (Eds.), Properties and Application of Perovskite-Type oxides, Marcel Dekker Inc., New York, 1992.
[15] W.S. Ahn, N.K. Kim, S.Y. Jeong, Catal. Today 68 (2001) 83.
[16] L.Y. Chen, G.K. Chuah, S. Jaenicke, J. Mol. Catal. A 132 (1998) 281.
[17] K. Chaudhari, R. Bal, D. Srinivas, A.J. Chandwadkar, S. Sivasanker, Microporous Mesoporous Mater. 50 (2001) 209.
[18] K. Chaudhari, R. Bal, A.J. Chandwadkar, S. Sivasanker, J. Mol. Catal. A 177 (2002) 247.
[19] K. Chaudhari, T.K. Das, A.J. Chandwadkar, S. Sivasanker, J. Catal. 186 (1999) 81.
[20] K.S.W. Sing, D.H. Everett, R.A. Haul, L. Moscow, R.A. Pierotti, J. Rouquerol, T. Siemieniewska, Pure Appl. Chem. 57 (1985) 603.
[21] M.G. Song, J.Y. Kim, S.H. Cho, J.D. Kim, Langmuir 18 (2002) 6110.
[22] M. Meng, P.Y. Lin, Y.L. Fu, Catal. Lett. 48 (1997) 213.
[23] V.M. Jiméne Z, J.P. Espinós, A.R. González-Elipe, Surf. Interface Anal. 26 (1998) 62.
[24] G.P. Huffman, N. Shan, J. Zhao, J. Catal. 151 (1995) 17.
[25] H.W. Xiang, T.D. Hu, B. Zhong, S.Y. Peng, Y.N. Xie, D.X. Huang, X.N. Chen, Chin. J. Chem. Phys. 8 (1995) 75.
[26] M.G. Sanchez, J.L. Gazquez, J. Catal. 104 (1987) 120.